INVESTIGATION OF CHAOTIC FORCED BENDING VIBRATIONS OF THE AUTOMOTIVE DRIVESHAFT

Mihai BUGARU[1], Andrei VASILE[2]

To investigate the chaotic forced bending vibrations of the automotive driveshaft it is necessary first to adopt an appropriate dynamic model that describes such dynamic behavior. Such a dynamic model was already realized in previous works by the authors, and therefore based on the dynamic equations already obtained it was used a complex method developed by the authors based on two elements: chaos manifestation detection, and chaos manifestation confirmation. The chaotic manifestation detection consists in using the time-history graphs in a specific resonance region namely the principal parametric region. For the same region was applied the Maximum Lyapunov Exponents Method (MLEM) was coupled with the contraction criterion for the sum of Lyapunov exponents that certifies the chaos. In addition, was applied the Poincaré Map as a qualitative method to reconfirm chaos manifestation. Thus, a powerful analytical tool was created to investigate the chaotic forced bending vibrations for specific conditions in the principal parametric resonance's area (PPRA).

Keywords: chaotic forced bending vibrations, time-history graphs, Lyapunov exponents, Poincaré Map, principal parametric resonance's area

1. Introduction

The paper represents a development of previous research carried out by the authors [1-3] concerning the dynamic behavior of automotive driveshafts. The automotive driveshafts are homokinetic transmission elements for cars from gearboxes or differential boxes to the wheels, being important elements of the automotive's driveline. The authors have already shown that geometric and kinematic isometry of the automotive driveshafts have nonuniformities [1] and therefore, all the dynamic models must consider this aspect [2], [3]. The present paper considers the same dynamic model for the forced bending vibrations of the automotive driveshaft, as in [3], involving the following physical aspects:

a. geometric and kinematic nonuniformities from the isometry property of the tulip, bowl, and midshaft as elements of the driveshaft;
b. due to the rigidity imposed by technical demands the tulip and the bowl have rigid body deflections and rotations($w_1 / w_3, \phi_1 / \phi_3, \varphi_1 / \varphi_3$ -

[1] Prof., Dept. of Mechanics, University POLITEHNICA of Bucharest, Romania, e-mail:skmbugaru@yahoo.com
[2] Eng., Expleo Group, Romania, e-mail: vasile_m_andrei@yahoo.com

tulip/bowl deflections and rotations, as shown in figure 1, while the midshaft is considered as a continuum media namely as a simply supported Timoshenko beam with mass, springs, and dampers at both ends having continuous functions w_2, ϕ_2, φ_2 respectively midshaft deflections and rotations;

c. the excitations are induced by the impact road shocks transmitted through automotive wheels generated by road nonuniformities [4].

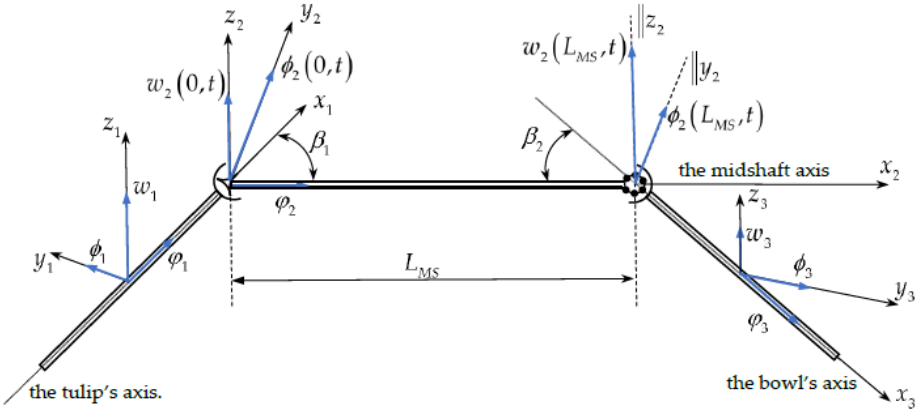

Fig. 1. Schematic representation of the deflections/rotations of the driveshaft elements[3]

Based on Hamilton's principle, [3] it was derived the forced bending vibrations equations using the previous assumptions. Starting from this point the present paper's analysis is devoted to detecting and certifying chaotic FBV (forced bending vibrations) for the automotive driveshaft elements in the PPRA (principle parametric resonance's area). Mazzei and Scott analyze in [5] the nonlinear dynamic behavior of automotive driveshaft elements in the PPRA. The experimental confirmation that one of the most important resonance areas for the FBV of automotive driveshafts is the PPRA was done by Steinwede in [6].

The detection of chaotic FBV in the PPRA will be performed using the general equations of FBV for a heavy-duty automotive driveshaft designed for an SUV (sports utility vehicle) having a permanent 4-WD (four-wheeler drive). This will imply the determination of the phase portraits for the tulip and the bowl in the PPRA. The certification of chaotic FBV manifestation in the PPRA implies the computation of Lyapunov exponents, namely the use of the Maximum Lyapunov Exponents Method (MLEM) for a modified system of equations for FBV of the automotive driveshaft elements (tulip and bowl) followed using the contraction criterion: *the sum of all Lyapunov exponents is negative* for tulip/bowl, as stated in [7]. As a supplementary confirmation of chaotic FBV manifestation for the tulip/bowl in the PPRA, it was computed Poincaré Maps for the tulip/bowl in the PPRA so that the pictures of Poincaré Maps have the property of *the system's*

auto-similarity, also mentioned in [7] as a qualitative method for chaos manifestation.

2. The Equations of FBV for the tulip/bowl of the automotive driveshaft

To calculate the equations of FBV for the tulip/bowl of the automotive driveshaft it is mandatory to reduce the mass inertial moments and the geometric inertial moments of the tulip/bowl to the cartesian system of reference (CSR) $X_2Y_2Z_2$ of the midshaft as in [3]. All the inertial characteristics of the tulip and the bowl, respecting the schematic representation shown in Figure 1, are presented in Appendix A, as described in the paper [3]. The dynamic model of FBV for the tulip is presented in Appendix B, while the dynamic model of FBV for the bowl is presented in Appendix C, being adopted with those stated in the paper [3]. The equation of the FBV in normalized bending deflection for the tulip is[3](pp. 13, 14)

$$\ddot{w}_1 + 2\xi\Omega_1\sqrt{\frac{1-C_1\cos(2\varphi_1)}{1-C_2\cos(2\varphi_1)}}\dot{w}_1 + \Omega_1^2\frac{1-C_1\cos(2\varphi_1)}{1-C_2\cos(2\varphi_1)}w_1 = -\Gamma_1 w_1^3 - \Gamma_2 w_1^5, \quad (1)$$

while the equation of the FBV in normalized bending deflection for the bowl is[3] (pp. 13, 14)

$$\ddot{w}_3 + 2\xi\Omega_3\sqrt{\frac{1-C_3\cos(2\varphi_3)}{1-C_4\cos(2\varphi_3)}}\dot{w}_3 + \Omega_3^2\frac{1-C_3\cos(2\varphi_3)}{1-C_4\cos(2\varphi_3)}w_3 = -\Gamma_3 w_3^3 - \Gamma_4 w_3^5. \quad (2)$$

The constants C_i, Γ_i and the natural frequencies for the tulip in bending Ω_1 and for the bowl in bending Ω_3 are expressed in Appendix D as stated in the paper [3]. The terms that induce the forced excitations in the PPRA contain for the tulip Ω_1, $\cos(2\varphi_1)$ and for the bowl Ω_3, $\cos(2\varphi_3)$ and must satisfy the equations [8](pp. 199, 425)

$$\eta_1 \square 2\Omega_1 \square \frac{2d\varphi_1}{dt}, \eta_3 \square 2\Omega_3 \square \frac{2d\varphi_3}{dt}, \quad (3)$$

where η_1 is the tulip's excitation frequency and η_3 is the bowl's excitation frequency. To use equations (1) and (2) it is mandatory to compute the tulip's geometry characteristics J_{1T}, J_{2T}, and the bowl's geometry characteristics J_{1B}, J_{2B} based on their general geometry. This was done using the AUTOCAD software, and the results presented in Table 1 are like the data in [3](pp. 15,19). Also, Table 1

Table 1

Tulip's/Bowl's geometry characteristics and material properties &shock's amplitude/time

$0.5(J_{1T}+J_{2T})$ [m^4]	$0.5(J_{1B}+J_{2B})$ [m^4]	χ_{nT} / χ_{nB}	ρ [kg/m^3]	E/G [GPa]	ξ	$\bar{F}_s$ / Δt_s [MN/ms]
9.1531×10^{-7}	10.560×10^{-7}	0.25/0.10	7850	200/77.3	$(16\text{-}318)10^{-4}$	0.5/1…10

illustrates the material properties of the tulip/bowl as well as the values of the shock's amplitude and the shock's duration. Comparing the data in Table 1 with those used by Steinwede in his experiments [6](p. 111) it can be remarked the agreements.

3. The Detection of Tulip's/Bowl's chaotic FBV in the PPRA

For the tulip, based on the relations (D1)(see Appendix D), the PPRA is defined by a range around the value 1038.38 Hz, the natural bending frequency being $\nu_1 = 519.19\,\text{Hz}$[3](pp. 19-20). Based on the relations (D2) (see Appendix D), for the bowl, the bowl's PPRA is defined by a range around the value 6306.6 Hz, the natural bending frequency being $\nu_3 = 3153.3\,\text{Hz}$[3](pp. 19-20). To determine the time phase portraits for the tulip and the bowl in FBV is mandatory to modify the equations (1) and (2), which become the systems

$$\begin{cases} \dfrac{dw_1}{dt} = V_{w_1}, \\ \dfrac{d\Theta_1}{dt} = \dfrac{d\theta_1}{dt} = \eta_1, \Theta_1 = \theta_1, \\ \dfrac{dV_{w_1}}{dt} = -2\xi\Omega_1\sqrt{\dfrac{1 - C_1 cos(\Theta_1)}{1 - C_2 cos(\Theta_1)}}V_{w_1} - \Omega_1^2\dfrac{1 - C_1 cos(\Theta_1)}{1 - C_2 cos(\Theta_1)}w_1 - \Gamma_1 w_1^3 - \Gamma_2 w_1^5, \end{cases} \tag{4}$$

$$\begin{cases} \dfrac{dw_3}{dt} = V_{w_3}, \\ \dfrac{d\Theta_3}{dt} = \dfrac{d\theta_3}{dt} = \eta_3, \Theta_3 = \theta_3, \\ \dfrac{dV_{w_3}}{dt} = -2\xi\Omega_3\sqrt{\dfrac{1 - C_3 cos(\Theta_3)}{1 - C_4 cos(\Theta_3)}}V_{w_3} - \Omega_3^2\dfrac{1 - C_3 cos(\Theta_3)}{1 - C_4 cos(\Theta_3)}w_3 - \Gamma_3 w_3^3 - \Gamma_4 w_3^5. \end{cases} \tag{5}$$

Using the MATLAB software, it was computed the time phase portraits of the tulip's FBV and the bowl's FBV in the PPRA are presented in Figures 2-5. Analyzing the phase portraits of the tulip's FBV (see Fig. 2.b, Fig. 3.b) it can be concluded that a chaotic FBV for the tulip is manifested in the range $\xi = 0.0016 - 0.0216$ of the damping ratio, while the increase with 0.02 of the damping ratio induces a decrease of the tulip's bending deflection w_1 more than ten times. Also, the same increase of the damping ratio induces a decrease of the tulip's velocity bending deflection $\dfrac{dw_1}{dt}$ more than six times. Analyzing the time

history of the tulip's phase portraits in the PPRA(see Fig. 2.a and 3.a) it is obvious the manifestations of beating effects specific to chaos.

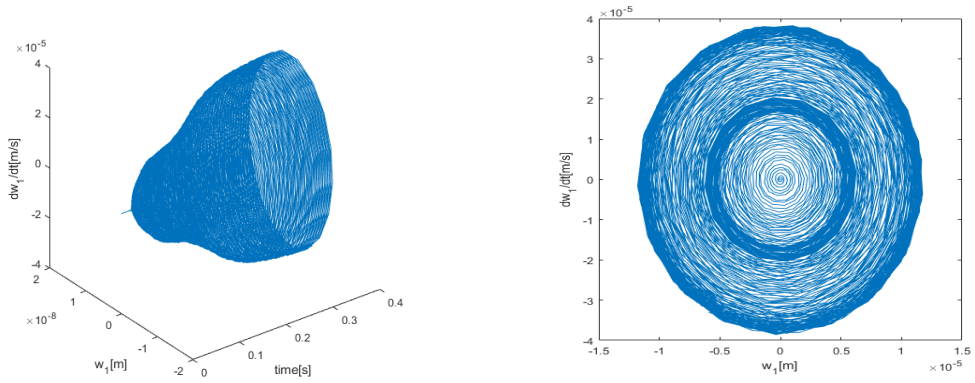

a. b.

Fig. 2. Time-history (phase portraits) of the tulip's FBV. $\chi_{nT} = 0.25, \xi = 0.0016$

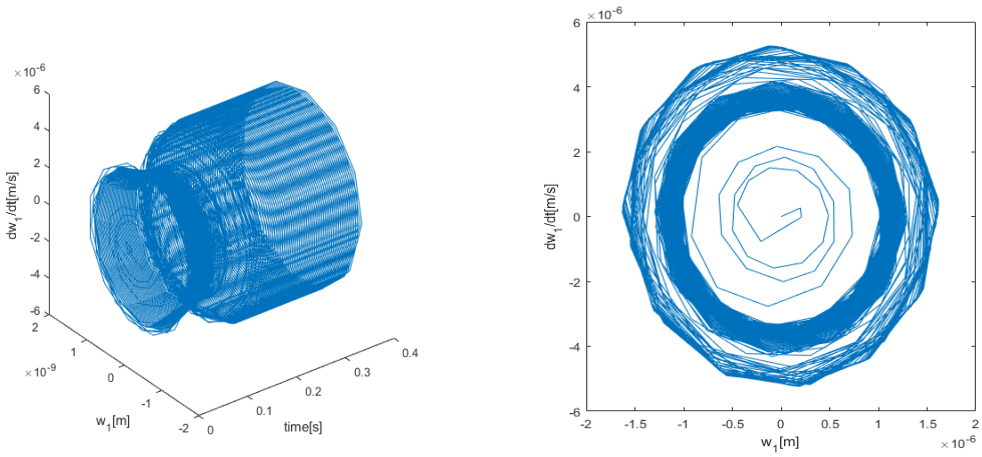

a. b.

Fig. 3. Time-history (phase portraits) of the tulip's FBV. $\chi_{nT} = 0.25, \xi = 0.0216$

Analyzing the phase portraits of the bowl's FBV (see Fig. 4.b, Fig. 5.b) it can be concluded that a chaotic FBV for the bowl is manifested in the same range $\xi = 0.0016 - 0.0216$ of the damping ratio, while the increase with 0.02 of the damping ratio induces a decrease of the bowl's bending deflection w_3 more than ten times. Also, the same increase of the damping ratio induces a decrease of the bowl's velocity bending deflection $\frac{dw_3}{dt}$ more than six times. Analyzing the time

history of the bowl's phase portraits in the PPRA (see Fig. 4.a and 5.a) it is obvious the manifestations of beating effects specific to chaos.

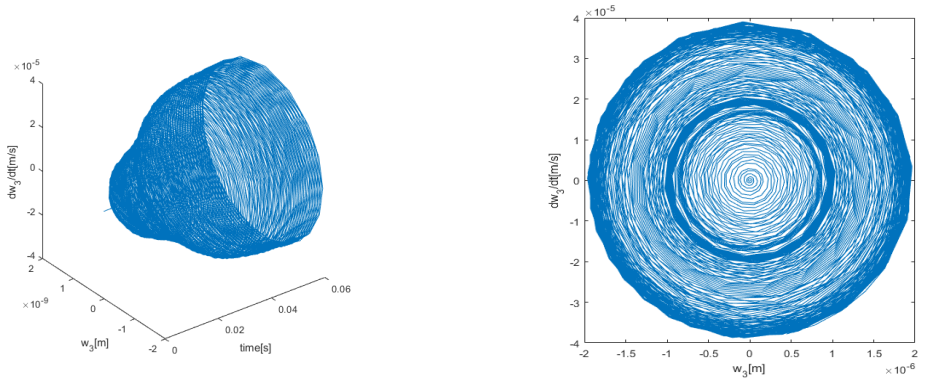

a. b.

Fig. 4. Time-history (phase portraits) of the bowl's FBV. $\chi_{nB} = 0.10, \xi = 0.0016$

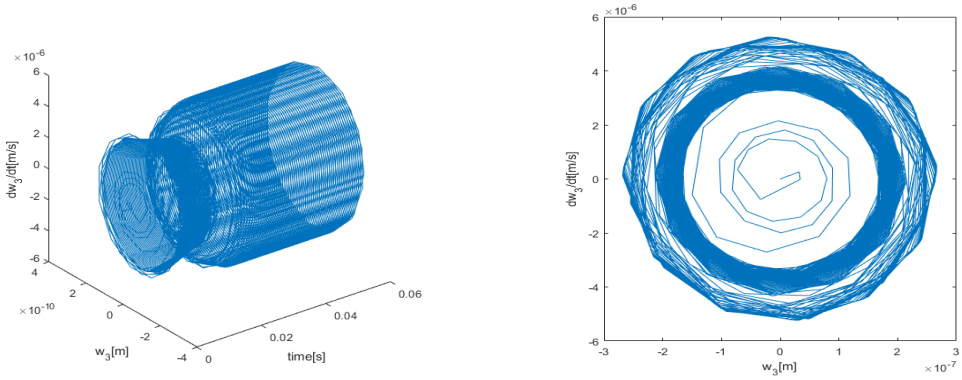

a. b.

Fig. 5. Time-history (phase portraits) of the bowl's FBV. $\chi_{nB} = 0.10, \xi = 0.0216$

If we compare the results illustrated in Figs. 2 and 3 for the tulip's FBV with those illustrated in Figures 4 and 5 for the bowl's FBV it can be remarked an accentuation of the beating effects for the bowl for the damping ratio around the value 0.0016 (see Fig. 2.b and Fig, 4.b) and a similar manifestation of time-history for the tulip's FBV and the bowl's FBV for the damping ratio around the value 0.0216 (see Fig. 3.a and Fig.5.a).

4. The Confirmation of the chaotic FBV for the tulip/bowl in PPRA

The Lyapunov exponents computed based on the system (4), that describes the tulip's FBV in the tulip's PPRA (the excitation frequency of the tulip is in the range around 1038.38 Hz[3]) are given by the equations [7](p. 306-307)

$$L_{11}=\frac{1}{T_f}\sum_{i=1}^{N} log_{10}\frac{\left|\left(w_1-w_1^p\right)^{Ti}\right|}{\left\|\left(w_1,V_{w_1},\Theta_1\right)^{Tf}-\left(w_1^p,V_{w_1}^p,\Theta_1^p\right)^{Tf}\right\|}, L_{21}=\frac{1}{T_f}\sum_{i=1}^{N} log_{10}\frac{\left|\left(V_{w_1}-V_{w_1}^p\right)^{Ti}\right|}{\left\|\left(w_1,V_{w_1},\Theta_1\right)^{Tf}-\left(w_1^p,V_{w_1}^p,\Theta_1^p\right)^{Tf}\right\|}, \quad (6)$$

$$L_{31}=\frac{1}{T_f}\sum_{i=1}^{N} log_{10}\frac{\left|\left(\Theta_1-\Theta_1^p\right)^{Ti}\right|}{\left\|\left(w_1,V_{w_1},\Theta_1\right)^{Tf}-\left(w_1^p,V_{w_1}^p,\Theta_1^p\right)^{Tf}\right\|},$$

where the superscript p indicates the perturbed solution on an interval break (T_i, T_{i+1}), T_f is the final time of integration and N is the number of intervals contained in the time range (0, T_f). The Lyapunov exponents computed based on the system (5), that describes the bowl's FBV in the bowl's PPRA (the excitation frequency of the bowl is in the range around 6306.6 Hz[3]) are given by the similar equations, with the same signification of the superscripts previously described,

$$L_{13}=\frac{1}{T_f}\sum_{i=1}^{N} log_{10}\frac{\left|\left(w_3-w_3^p\right)^{Ti}\right|}{\left\|\left(w_3,V_{w_3},\Theta_3\right)^{Tf}-\left(w_3^p,V_{w_3}^p,\Theta_3^p\right)^{Tf}\right\|}, L_{23}=\frac{1}{T_f}\sum_{i=1}^{N} log_{10}\frac{\left|\left(V_{w_3}-V_{w_3}^p\right)^{Ti}\right|}{\left\|\left(w_3,V_{w_3},\Theta_3\right)^{Tf}-\left(w_3^p,V_{w_3}^p,\Theta_3^p\right)^{Tf}\right\|}, \quad (7)$$

$$L_{33}=\frac{1}{T_f}\sum_{i=1}^{N} log_{10}\frac{\left|\left(\Theta_1-\Theta_1^p\right)^{Ti}\right|}{\left\|\left(w_3,V_{w_3},\Theta_3\right)^{Tf}-\left(w_3^p,V_{w_3}^p,\Theta_3^p\right)^{Tf}\right\|}.$$

To certify the chaos is necessary to apply two criteria respectively the Maximum Lyapunov Exponents Method (MLEM) coupled with the contraction criterion of the sum of all Lyapunov exponents that imposes the next mathematical proposition to be true [7](pp. 306-307), [9]

$$\exists i\subset\{1,2,3\}, max(L_{ij})\rangle 0, \exists L_{ij}\approx 0, \sum_{1}^{3} L_{ij}\langle 0, j\subset\{1,2,3\}. \quad (8)$$

Figures 6 and 7 are illustrated the Lyapunov exponents for two values of the damping ratio 0.0016 and 0.011 in the tulip's PPRA, with excitation frequency in the vicinity of 1038.38 Hz. As can be remarked from Figures 6 and 7 the proposition (8) is true only for the damping ratio in the range of 0.0016-0.011. Analyzing Figure 6 it can be concluded that chaos manifestation is confirmed in the excitation frequency range (950-1150) Hz for the damping ratio of 0.0016, while in Figure 7 the chaos manifestation is confirmed in the excitation frequency range (1100-1150) Hz for the damping ratio of 0.011 even if from chaos detection (see Fig. 3) it indicates the maximum value of damping ratio 0.0216. Figures 8 and 9 are illustrated the Lyapunov exponents for two values of the damping ratio 0.0016 and 0.0125 in the bowl's PPRA, with excitation frequency in the vicinity of 6306.6 Hz.

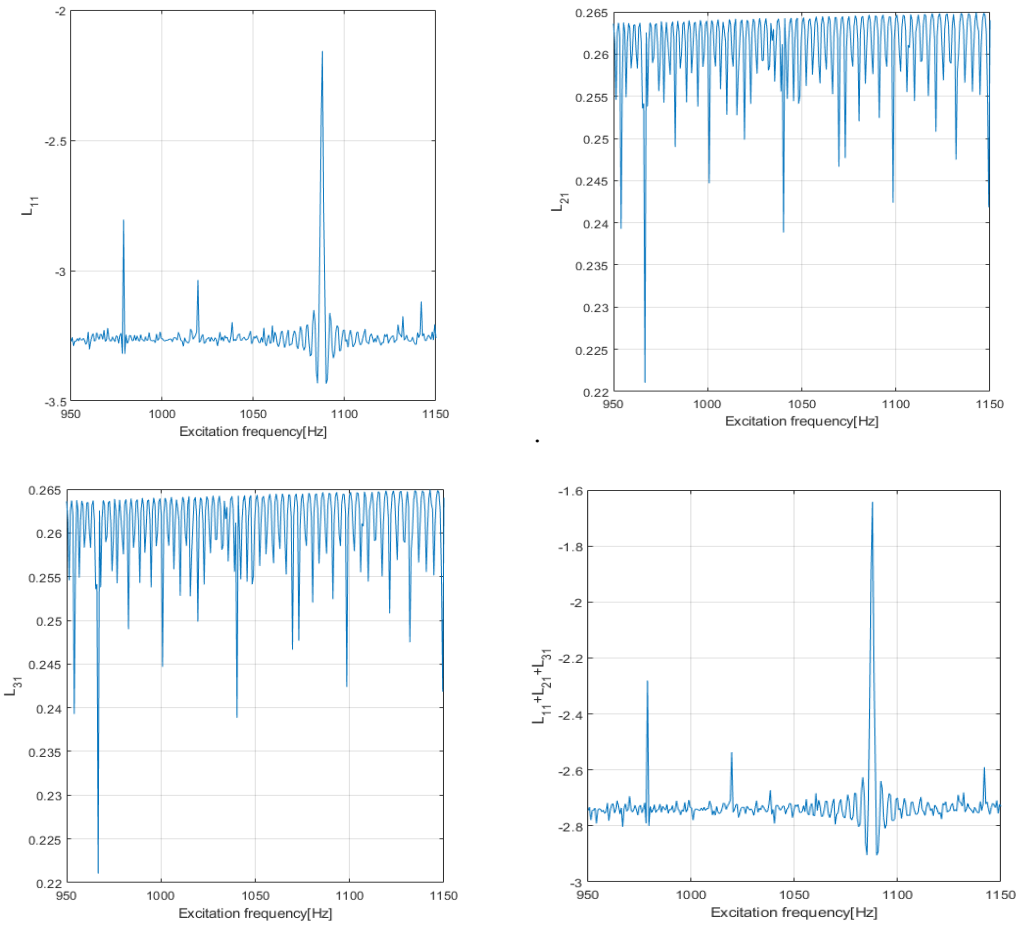

Fig. 6. Tulip's Lyapunov exponents of FBV in the PPRA(1038.38Hz), $\nu_1 = 519.19\,\text{Hz}$, $\xi = 1.6 \cdot 10^{-3}$

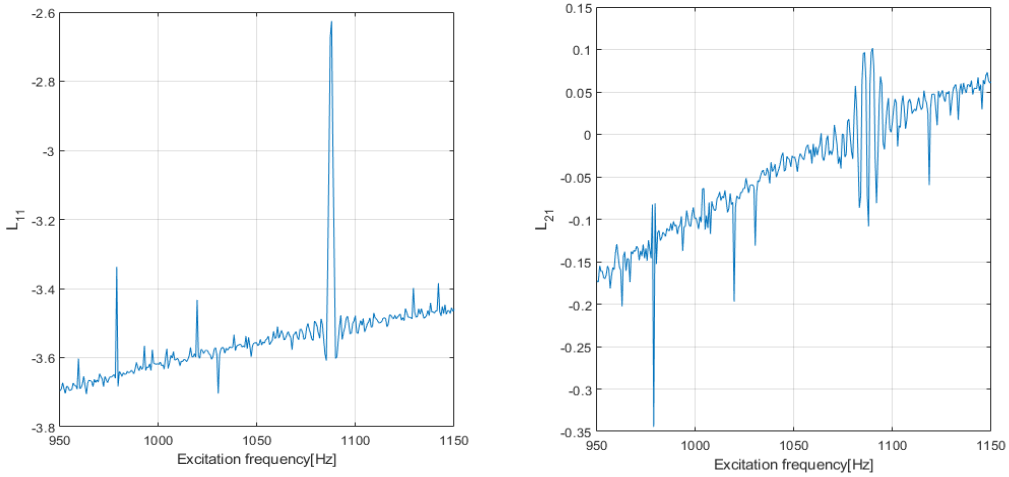

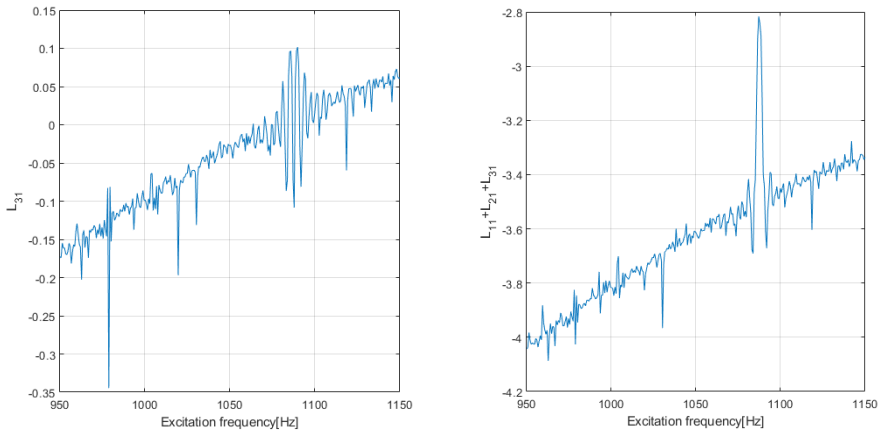

Fig. 7. Tulip's Lyapunov exponents of FBV in the PPRA(1038.38Hz), $\nu_1 = 519.19\,\text{Hz}$, $\xi = 11 \cdot 10^{-3}$

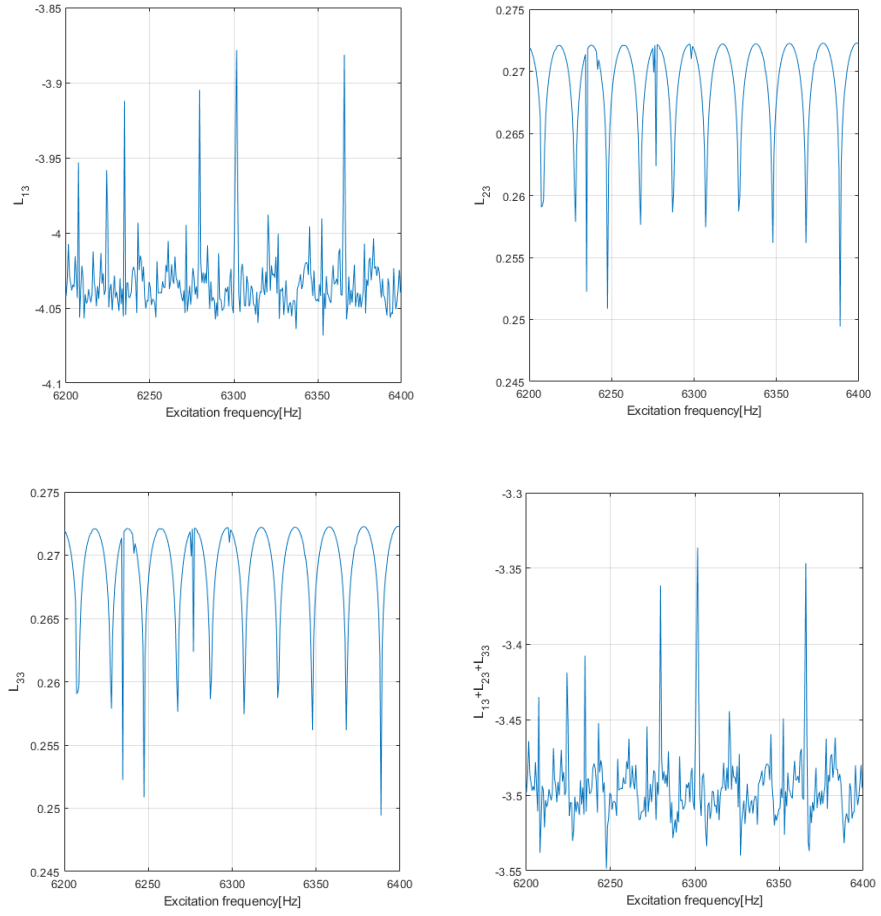

Fig. 8. Bowl's Lyapunov exponents of FBV in the PPRA(6306.6Hz), $\nu_3 = 3153.3\,\text{Hz}$, $\xi = 1.6 \cdot 10^{-3}$

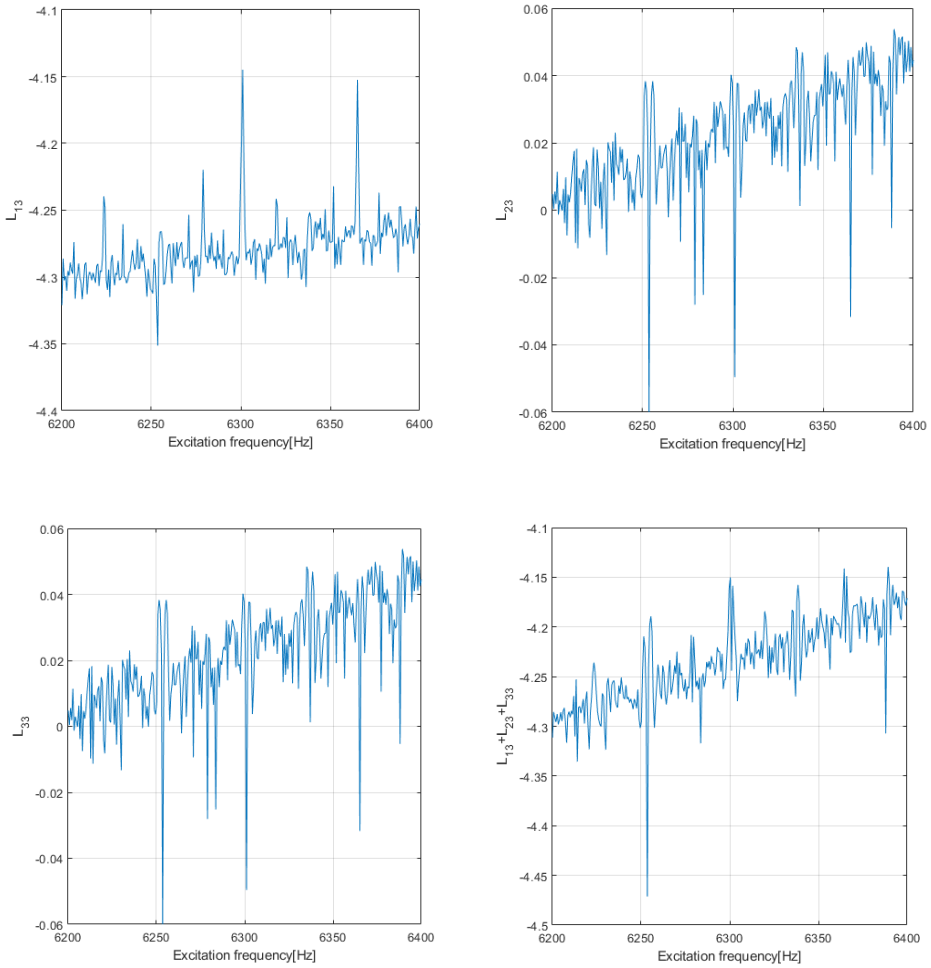

Fig. 9. Bowl's Lyapunov exponents of FBV in the PPRA(6306.6Hz), $\nu_3 = 3153.3$ Hz, $\xi = 12.5 \cdot 10^{-3}$

As can be remarked from Figs. 8 and 9 the proposition (8) is true only for the damping ratio in the range of 0.0016-0.0125. Analyzing Fig. 8 it can be concluded that chaos manifestation is confirmed in the excitation frequency range (6200-6400) Hz for the damping ratio of 0.0016, while in Fig. 9 the chaos manifestation is confirmed in the excitation frequency ranges (6300-6365) Hz and (6368-6400) Hz for the damping ratio of 0.0125 even if from chaos detection (see Fig. 5) it indicates the maximum value of damping ratio 0.0216. Accordingly, to the latest developments in the theory of chaos if two Lyapunov exponents are positive and all the Lyapunov exponents respect the proposition (8) the dynamic system is consider to be a hyperchaotic system [10]. Analyzing Figures 6-9 it can be concluded that the automotive driveshaft is a hyperchaotic system for a damping ratio in the range of 0.0016-0.011 and excitation frequency in the range (1100-1150)Hz for the tulip in FBV, while for the bowl in FBV the hyperchaos

manifestation is valid for a damping ratio in the range of 0.0016-0.0125 and excitation frequency in the ranges (6300-6365) Hz and (6368-6400)Hz. To reconfirm the chaotic manifestation of tulip's FBV and bowl's FBV in the PPRA it was computed, using in MATLAB software based on systems (4) and (5), the Poincaré Maps (PM) that represents the intersection of the orbits in the phase portraits with an orthogonal surface at equal periods (N number of points), using the mathematical procedure presented in [7] (p. 194). If the tulip's FBV or the bowl's FBV are periodic or quasi-periodic the PM represent saddle points or saddle separatrices pictures. For an excitation frequency range in the vicinity of 1038.38 Hz and for a damping ratio $\xi = 1.6 \cdot 10^{-3}$ Fig. 10 illustrates the Poincaré Map for the tulip's FBV in the PPRA using N =100,000 orthogonal surface sections to the orbits for the phase portraits $\left(w_1, dw_1 / dt\right)$.

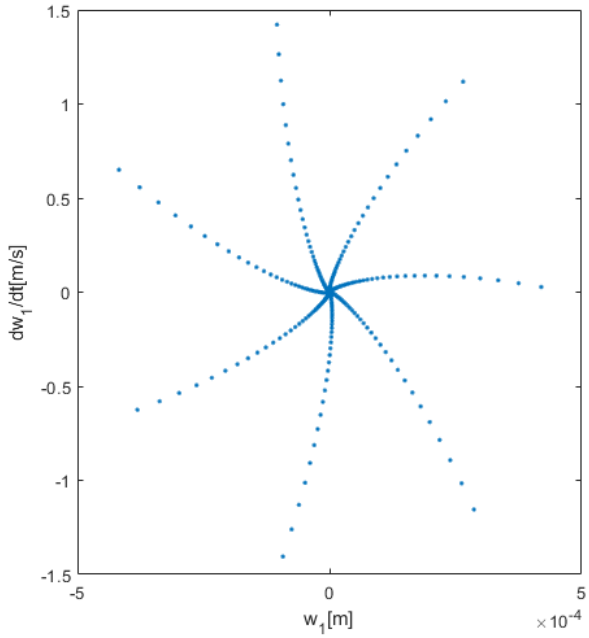

Fig. 10. Poincaré Map for the tulip's FBV in the PPRA(1038.38Hz), N=100,000 $\xi = 1.6 \cdot 10^{-3}$

As can be remarked from Figure 10 the picture has the properties of strange attractors respectively auto-similarity and a diffuse structure of points having a different density of pixels per image's unit area.

For an excitation frequency range in the vicinity of 6306.6 Hz and for a damping ratio $\xi = 1.6 \cdot 10^{-3}$ Fig. 11 illustrates the Poincaré Map for the bowl's FBV in the PPRA using N =100,000 orthogonal surface sections to the orbits for the phase portraits $\left(w_3, dw_3 / dt\right)$.

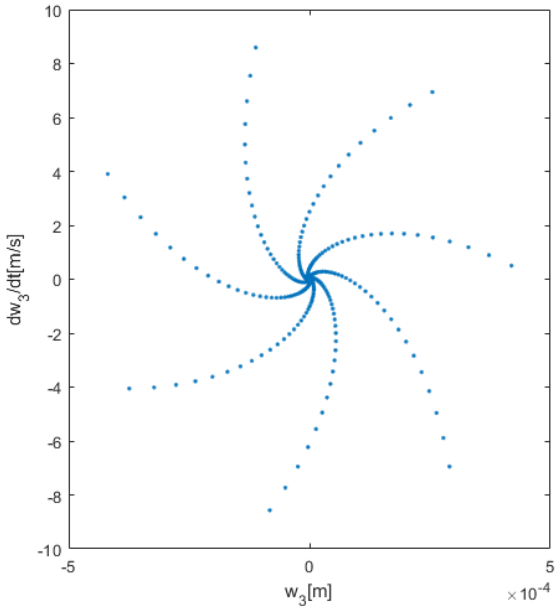

Fig. 11. Poincaré Map for the bowl's FBV in the PPRA(6306.6Hz), N=100,000 $\xi = 1.6 \cdot 10^{-3}$

As can be remarked from Fig. 11 the picture has the properties of strange attractors respectively auto-similarity and a diffuse structure of points having a different density of pixels per image's unit area. The reconfirmation of chaotic manifestation of the tulip's and bowl's FBV through Poincaré Maps respectively the strange attractors. Such dynamic behavior is considered by Steinwede [6](pp. 88-94) to be the cause of the internal pitting of the bells of the tulip and the bowl as well as the micro-cracks on the tripod axes. Also, Steinwede assimilated the mechanism of the chaotic FBV and chaotic forced torsional vibration of the automotive driveshafts with a similar mechanism for the nonlinear dynamic behavior of the geared systems transmissions, mechanisms already investigated by the first author of the present paper in [11]. As can be remarked the increase of the damping ratio has a benefic effect avoiding the chaotic behavior of FBV for the automotive driveshafts but it induces thermal stress.

5. Conclusions

The novelty of this paper is that investigated the chaotic FBV of the automotive driveshafts using a new method with two steps: detection of possible chaotic manifestation using phase portraits time-history and quantitative and qualitative confirmation of the deterministic chaos (strange attractors) for FBV using a modified MLEM coupled with Poincaré Maps. The results obtained confirmed theoretically for the first time the manifestation of FBV's hyperchaos

in the principal parametric resonance area for the tulip and the bowl agreeing with the Steinwede's experimental research [6](pp. 86-94) for the pitting manifestation, as well as the data referring to mass moment of inertia[6](p. 111) and the chaotic dynamic behavior of homokinetic transmission similar with the chaotic dynamic behavior of the geared transmission [6](p. 117), chaotic mechanism already studied by the first author in [11]. Finally, the paper highlighted the mechanism of hyperchaotic nonlinear dynamic behavior for the homokinetic transmission[10]. This new method may be used as a powerful tool by the designers of automotive driveshafts as well as the designers of the FBV's dynamic absorbers for the automotive driveshafts.

Acknowledgments

This work has been funded by the European Social Fund from the Sectoral Operational Programme Human Capital 2014-2020, through the Financial Agreement with the title "Training of Ph.D. students and postdoctoral researchers in order to acquire applied research skills - SMART", Contract no. 13530/16.06.2022 - SMIS code: 153734.

REFERENCES

[1]. *M. Bugaru, A. Vasile*, "Nonuniformity of Isometric Properties of Automotive Driveshafts", in Computation-MDPI, **vol. 9**, no. 145, Dec. 2021, pp. 1-13

[2]. *M. Bugaru, A. Vasile*, "A Physically Consistent Model for Forced Torsional Vibrations of Automotive Driveshafts", in Computation-MDPI, **vol. 10**, no. 10, Jan. 2022, pp. 1-21

[3]. *M. Bugaru, O. Vasile*, "Modeling and Analysis of FBV Movements for Automotive Driveshafts", in Applied Sciences-MDPI, **vol. 12**, no. 3237, March. 2022, pp. 1-35

[4]. *T. Sireteanu, O. Gündisch, S. Părăian,* Vibrațiile aleatoare ale automobilelor (Random vibrations of automobiles), Editura tehnică, Bucureşti, 1981.

[5]. *A.J.Jr. Mazzei, R.A. Scott*, "Principal parametric resonance zones of a rotating rigid shaft driven through a universal joint. Journal of Sound and Vibration". **vol. 244**, no. 3, July 2001, pp. 555–562.

[6]. *J. Steinwede*, Design of a Homokinetic Joint for Use in Bent Axis Axial Piston Motors. Ph.D. Thesis, Aachen University, Aachen, Germany, 2020.

[7]. *E. Deciu, M. Bugaru, Cr. Dragomirescu,* Vibrații Nelinare cu Aplicații în Ingineria Mecanică (Nonlinear Vibrations with Applications in Mechanical Engineering), Editura Academiei Române, Bucureşti, 2002.

[8]. *A.H. Nayfeh, D.T. Mook,* Nonlinear Oscillations, John Wiley & Sons: New York, NY, USA, 1979.

[9]. *J. Lou, S. Zhu*, "Three Conditions Lyapunov Exponents Should Satisfy", in Proceedings of the DETC'03, ASME Design Engineering, Technical Conferences and Computers and Information in Engineering Conference, Chicago, IL, USA, 2–6 Sept. 2003, pp. 1–4.

[10]. *S. Li, Y. Wu, X. Zhang,* "Analysis and Synchronization of a New Hyperchaotic System with Exponential Term", in Mathematics-MDPI, **vol. 9**, no. 3281, Dec. 2021, pp. 1-16

[11]. *M. Bugaru,* "Chaotic Behavior of Helical Gear-Pair Systems Non-linear Parametrically Excited", in Romanian Journal of Acoustics and Vibration, vol. 1, no.1, Dec. 2004, pp. 7–13.

Appendix A. The Inertial characteristics of the tulip/bowl driveshaft[3]

"The geometric inertial moments J_{Y_2T}, J_{Z_2T} and the mass inertial moments I_{Y_2T}, I_{Z_2T} of the tulip reduced to the midshaft axes Y_2, Z_2 are

$$J_{Y_2T} = J_{Y_2TB} + J_{Y_2TA},\ J_{Z_2T} = J_{Z_2TB} + J_{Z_2TA},\ I_{Y_2T} = J_{Y_2TB}\rho L_{TB} + J_{Y_2TA}\rho L_{TA},\ I_{Z_2T} = J_{Z_2TB}\rho L_{TB} + J_{Z_2TA}\rho L_{TA}, \tag{A1}$$

$$J_{Y_2TB} = 0.5\left(J_{1T} + J_{2T}\right)\left[1 + sin^2\beta_1 + \chi_{nT}\cos\left(2\varphi_1\right)cos^2\beta_1\right] + \frac{S_T L_{TB}^2}{12}cos^2\beta_1 + S_T\left(d_{CT}\right)^2, \tag{A2}$$

$$J_{Y_2TA} = \frac{\pi d_{TA}^4}{64}\left(1 + sin^2\beta_1\right) + \frac{\pi d_{TA}^2}{4}\frac{L_{TA}^2}{12}cos^2\beta_1 + \frac{\pi d_{TA}^2}{4}\left(L_{TB} + 0.5L_{TA}\right)^2,\ \chi_{nT} = \frac{J_{1T} - J_{2T}}{J_{1T} + J_{2T}}, \tag{A3}$$

$$J_{Z_2TB} = 0.5\left(J_{1T} + J_{2T}\right)\left[1 - \chi_{nT}\cos\left(2\varphi_1\right)\right] + \frac{S_T L_{TB}^2}{12} + S_T\left(d_{CT}\right)^2,\ J_{Z_2TA} = \frac{\pi d_{TA}^4}{64} + \frac{\pi d_{TA}^2}{4}\frac{L_{TA}^2}{12} + \frac{\pi d_{TA}^2}{4}\left(L_{TB} + 0.5L_{TA}\right)^2, \tag{A4}$$

where J_{1T}, J_{2T} are the principal geometric moments of inertia for the tulip's bell, $J_{Y_2TB}, J_{Y_2TA}, J_{Z_2TB}, J_{Z_2TA}$ are the geometric moments of inertia for the tulip's elements reduced to the axes Y_2, Z_2, ρ is the mass density of the automotive driveshaft elements, d_{CT} is the distance between the center mass of the tulip and the tripod's center mass, S_T is the surface of the cross-section for the tulip's bell, χ_{nT} is the nonuniformity of the geometric moments of inertia for the tulip, L_{TB} is the length of the tulip's bell, L_{TA} is the length of the tulip ax, and d_{TA} is the diameter of the tulip ax. The geometric inertial moments J_{Y_2B}, J_{Z_2B} and the mass inertial moments I_{Y_2B}, I_{Z_2B} of the bowl reduced to the midshaft axes Y_2, Z_2 are

$$J_{Y_2B} = J_{Y_2BB} + J_{Y_2BA},\ J_{Z_2B} = J_{Z_2BB} + J_{Z_2BA},\ I_{Y_2B} = J_{Y_2BB}\rho L_{BB} + J_{Y_2BA}\rho L_{BA},\ I_{Z_2B} = J_{Z_2BB}\rho L_{BB} + J_{Z_2BA}\rho L_{BA}, \tag{A5}$$

$$J_{Y_2BB} = 0.5\left(J_{1B} + J_{2B}\right)\left[1 + sin^2\beta_2 + \chi_{nB}\cos\left(2\varphi_3\right)cos^2\beta_2\right] + \frac{S_B L_{BB}^2}{12}cos^2\beta_2 + S_B\left(d_{CB}\right)^2, \tag{A6}$$

$$J_{Y_2BA} = \frac{\pi d_{BA}^4}{64}\left(1 + sin^2\beta_2\right) + \frac{\pi d_{BA}^2}{4}\frac{L_{BA}^2}{12}cos^2\beta_2 + \frac{\pi d_{BA}^2}{4}\left(L_{BB} + 0.5L_{BA}\right)^2,\ \chi_{nB} = \frac{J_{1B} - J_{2B}}{J_{1B} + J_{2B}}, \tag{A7}$$

$$J_{Z_2BB} = 0.5\left(J_{1B} + J_{2B}\right)\left[1 - \chi_{nB}\cos\left(2\varphi_3\right)\right] + \frac{S_B L_{BB}^2}{12} + S_B\left(d_{CB}\right)^2,\ J_{Z_2BA} = \frac{\pi d_{BA}^4}{64} + \frac{\pi d_{BA}^2}{4}\frac{L_{BA}^2}{12} + \frac{\pi d_{BA}^2}{4}\left(L_{BB} + 0.5L_{BA}\right)^2, \tag{A8}$$

with the same signification as previously but for the bowl."[3].

Appendix B. The Dynamic model for tulip-tripod joint[3]

The dynamic model for the FBV of the tulip, tulip-tripod joint and midshaft of the automotive driveshaft is illustrated in Figure B as presented in paper[3].

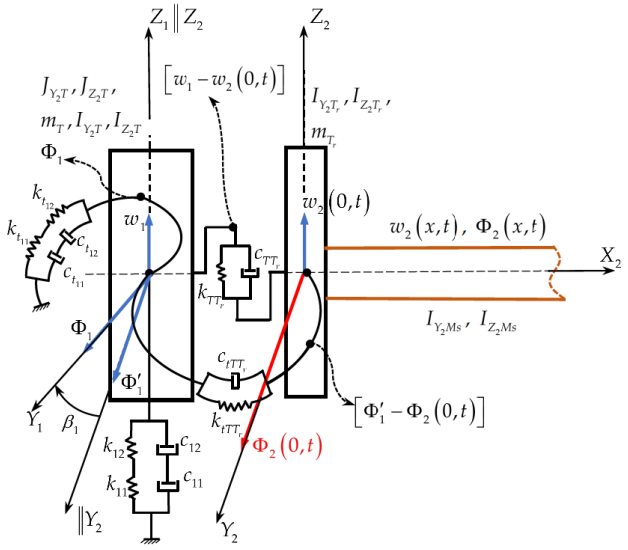

Fig. B. Dynamic model of FBV for: tulip, tulip-tripod joint, and midshaft[3].

"The tulip has a stiffness k_1, and damping c_1, for the bending vibration rigid movement of the tulip regarding the axis Z_2 and a stiffness k_{t1}, as well as damping c_{t1}, for the angular bending vibration rigid movement of the tulip regarding the axis Y_2, given by the following relations:

$$k_{11} = \frac{3EJ_{Z_2TA}}{L_{TA}^3}, k_{12} = \frac{3EJ_{Z_2TB}}{L_{TB}^3}, k_1 = \frac{k_{11}k_{12}}{k_{11}+k_{12}}, c_1 = \xi\sqrt{k_1 m_T}, \tag{B1}$$

$$k_{t1} = \frac{GJ_{Y_2TA}}{L_{TA}}, k_{t_{12}} = \frac{GJ_{Y_2TB}}{L_{TB}}, k_{t1} = \frac{k_{t_{11}}k_{t_{12}}}{k_{t_{11}}+k_{t_{12}}}, c_{t1} = \xi\sqrt{k_{t1} I_{Y_2T}}, \tag{B2}$$

where E is Young's modulus, G is the shearing modulus, m_T is the tulip's mass,"[3] and ξ is the damping ratio of the tulip's material (the same as bowl's material), that is steel (ξ=0.0016-0.0318) [7]. "The uniform midshaft (see Figures B, C) in continuous FBV movement is assimilated with a uniform Timoshenko beam simply supported at both ends by elastic supports (the tulip–tripod and inner race–bowl joints are elastic supports for the midshaft), having at $x = 0$ a tripod fixed on the midshaft through splines and elastically linked in the tulip–tripod joint with the tulip and on the left-hand side at $x = L_{Ms}$ an inner race (see Figure C)

fixed on the midshaft through splines and elastically linked in the bowl–inner race joint with the bowl, with the inertial characteristics given by the relations below:

$$J_{Y_2Tr} = 0.5\left(J_{1Tr} + J_{2Tr}\right)\left[1 + \chi_{nTr}\, cos\left(2\varphi_2\right)\right], J_{Z_2Tr} = 0.5\left(J_{1Tr} + J_{2Tr}\right)\left[1 - \chi_{nTr}\, cos\left(2\varphi_2\right)\right], \quad \text{(B3)}$$

$$J_{Y_2Ir} = 0.5\left(J_{1Ir} + J_{2Ir}\right)\left[1 + \chi_{nIr}\, cos\left(2\varphi_2\right)\right], J_{Z_2Ir} = 0.5\left(J_{1Ir} + J_{2Ir}\right)\left[1 - \chi_{nIr}\, cos\left(2\varphi_2\right)\right], \quad \text{(B4)}$$

where J_{1Tr}, J_{2Tr} are the principal geometric moments of inertia for the tripod, J_{1Ir}, J_{2Ir} are the principal geometric moments of inertia for the inner race, χ_{nTr} and χ_{nIr} are the geometric nonuniformities of the tripod and inner race, and $J_{Y_2Tr}, J_{Z_2Tr}, J_{Y_2Ir}, J_{Z_2Ir}$ are the geometric moments of inertia of the tripod and inner race concerning the axes Y_2, Z_2 ."[3]

Appendix C. The Dynamic model for bowl-inner race joint[3]

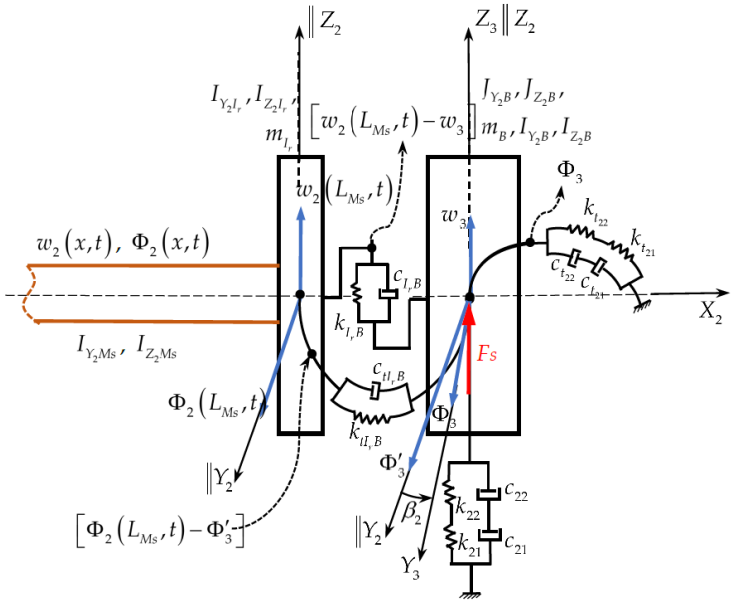

Fig. C. Dynamic model of FBV for: bowl, bowl-inner race joint, and midshaft[3].

"The bowl has a stiffness k_2, and damping c_2, for the bending vibration rigid movement of the bowl regarding the axis Z_2 and a stiffness k_{t2}, as well as damping c_{t2}, for the angular bending vibration rigid movement of the bowl regarding the axis Y_2, given by the following relations:

$$k_{21} = \frac{3EJ_{Z_2BA}}{L_{BA}^3}, k_{22} = \frac{3EJ_{Z_2BB}}{L_{BB}^3}, k_2 = \frac{k_{21}k_{22}}{k_{21} + k_{22}}, c_2 = \xi\sqrt{k_2 m_B}, \quad \text{(C1)}$$

$$k_{t_{21}} = \frac{GJ_{Y_2BA}}{L_{BA}}, k_{t_{22}} = \frac{GJ_{Y_2BB}}{L_{BB}}, k_{t2} = \frac{k_{t_{21}}k_{t_{22}}}{k_{t_{21}} + k_{t_{22}}}, c_{t2} = \xi\sqrt{k_{t2} I_{Y_2B}}, \quad \text{(C2)}$$

where m_B is the bowl's mass. The wheel induces excitations as a moderate impulsive shock force F_S acting in the Z_2 direction, and the excitation load can be expressed as

$$F_S = \overline{F}_S \left[1 + q_3 t^{q_1} e^{-q_2 t}\right], \tag{C3}$$

where $\overline{F}_S$ is the amplitude of the shock on the bowl's longitudinal axis X_3 transmitted from the wheel axis and $q_i, i = \overline{1,3,}$ are experimental constants, depending on the type of shock applied at the wheel by the road excitation [4]. All the computations were performed considering that the tulip was a cantilever beam fixed in the gearbox with simple elastic supports in the tulip–tripod joint. The bowl was a cantilever beam fixed in the steering wheel by simple elastic supports in the bowl–inner race joint. As mentioned in the literature [4], the shock excitation loads produce huge automotive stress solicitations in the car suspension system and the rim–tire system. These two systems can absorb 90% of the shock energy. Therefore, only 10% of the shock acts on the automotive driveshaft elements as a variation of the quantity of movement during a very short time, estimated at 0.001 s."[3]

Appendix D. Natural frequencies of the tulip/bowl and coefficients in the FBV's equations [3]

$$\Omega_1 = \sqrt{\frac{3E}{m_T L_{TA}^3} \frac{b_1(1+a_1)}{1+\frac{b_1}{J_{Z_2TA}}(1+a_1)}}, a_1 = \frac{0.5\left(J_{1T}+J_{2T}\right)}{S_T\left[\frac{L_{TA}^2}{12}+d_{CT}^2\right]}, b_1 = S_T\left[\frac{L_{TA}^2}{12}+d_{CT}^2\right], \tag{D1}$$

$$\Omega_3 = \sqrt{\frac{3E}{m_B L_{BA}^3} \frac{b_2(1+a_2)}{1+\frac{b_2}{J_{Z_2BA}}(1+a_2)}}, a_2 = \frac{0.5\left(J_{1B}+J_{2B}\right)}{S_B\left[\frac{L_{BA}^2}{12}+d_{CB}^2\right]}, b_2 = S_B\left[\frac{L_{BA}^2}{12}+d_{CB}^2\right], \tag{D2}$$

$$\Gamma_1 = \frac{0.2\rho A}{\pi 3!}\frac{\overline{F}_S \Delta t_s}{M m_T}\Omega_1, \Gamma_2 = \frac{0.2\rho A}{\pi 5!}\frac{\overline{F}_S \Delta t_s}{M m_T}\Omega_1, \Gamma_3 = \frac{0.2\rho A}{\pi 3!}\frac{\overline{F}_S \Delta t_s}{M m_B}\Omega_3, \Gamma_4 = \frac{0.2\rho A}{\pi 5!}\frac{\overline{F}_S \Delta t_s}{M m_B}\Omega_3, \tag{D3}$$

$$C_1 = \frac{a_1}{1+a_1}\chi_{nT}, C_2 = \frac{a_1 b_1}{J_{Z_2TA}+b_1\left(1+a_1\right)}\chi_{nT}, C_3 = \frac{a_2}{1+a_2}\chi_{nB}, C_4 = \frac{a_2 b_2}{J_{Z_2BA}+b_2\left(1+a_2\right)}\chi_{nB}, \tag{D4}$$

In the relations (D3) M is the suspended car mass distributed to one wheel, A is the cross-section area of the midshaft, Δt_s is the duration of the shock (impact) induced to the wheel. The relation (D1) expressed the tulip's natural frequency for FBV while the relation (D2) expressed the bowl's natural frequency for FBV.